Biomedical Materials

PURPOSE-LED PUBLISHING™

PAPER • OPEN ACCESS

Auxiliary electrode tunes wet-electrospun bundle stiffness to modulate cell phenotype

To cite this article: Haoyu Wang *et al* 2025 *Biomed. Mater.* **20** 045031

View the article online for updates and enhancements.

You may also like

- ICRH modelling of DTT in full power and reduced-field plasma scenarios using full wave codes
A Cardinali, C Castaldo, F Napoli et al.
- Borealization of tundra ecosystems with climate and land-use change
Mariana Verdonen, Isabel C Barrio, Laura Barbero-Palacios et al.
- Global evidence that cold rocky landforms support icy springs in warming mountains
Stefano Brighenti, Constance I Millar, Scott Hotaling et al.

This content was downloaded from IP address 144.82.114.255 on 07/01/2026 at 10:11

IOP Publishing Biomed. Mater. 20 (2025) 045031 https://doi.org/10.1088/1748-605X/ade8c6

Biomedical Materials

OPEN ACCESS

RECEIVED
16 January 2025

REVISED
9 May 2025

ACCEPTED FOR PUBLICATION
26 June 2025

PUBLISHED
18 July 2025

Original content from this work may be used under the terms of the Creative Commons Attribution 4.0 licence.

Any further distribution of this work must maintain attribution to the author(s) and the title of the work, journal citation and DOI.

PAPER

Auxiliary electrode tunes wet-electrospun bundle stiffness to modulate cell phenotype

Haoyu Wang[1], Chelsea Violita Stanley[1,2], Xiangshen Gao[3], Ziyu Liu[4], Mo Zhou[1], Mingjing Zhang[1], Feng-lei Zhou[5,6], Maryam Tamaddom[1] and Chaozong Liu[1,*]

[1] Division of Surgery & Interventional Science, University College London, Royal National Orthopaedic Hospital, Stanmore HA7 4LP, United Kingdom
[2] School of Chemistry, Chemical Engineering and Biotechnology, Nanyang Technological University, Singapore 637457, Singapore
[3] Beijing Key Laboratory of Advanced Manufacturing Technology, College of Mechanical and Energy Engineering, Beijing University of Technology, Beijing, People's Republic of China
[4] Beijing Advanced Innovation Centre for Biomedical Engineering, School of Engineering Medicine, Beihang University, Beijing 100191, People's Republic of China
[5] Centre for Medical Image Computing, Department of Medical Physics and Biomedical Engineering, University College London, London WC1V 6LJ, United Kingdom
[6] College of Textiles and Clothing, Qingdao University, Qingdao 266071, People's Republic of China
[*] Author to whom any correspondence should be addressed.

E-mail: chaozong.liu@ucl.ac.uk

Keywords: wet-electrospinning, auxiliary electrode, PCL, bundle, stiffness, cell morphology

Abstract

The stiffness of tissue-engineered scaffolds significantly influences cell behaviour and phenotype. However, current approaches to tuning stiffness often introduce unintended variations and compromise topographical consistency. In this study, an innovative wet-electrospinning set-up, incorporating a positively charged auxiliary electrode was developed to fabricate bundles with adjustable stiffness. COMSOL-based electromechanical computing revealed that the auxiliary electrode provided electrostatic force, which reduced stress concentration during continuous polycaprolactone (PCL) bundle collection at speeds up to 120 m min^{-1}. Tensile testing showed that increasing collection speed significantly enhanced bundle stiffness, with Young's modulus rising from 40 to 107 MPa. X-ray diffraction analysis indicated that this strengthen effect was associated with crystal disintegration and grain refinement within PCL fibre. These changes were reflected in scaffold stiffness, thereby, further influenced cell behaviour, as bundles with higher stiffness promoted a transition from non-polarised to spindle-like cell morphology. This electrostatic-assisted collection wet-electrospun setup enables the fabrication of scaffolds with tuneable mechanical properties while preserving topographical consistency, offering a robust strategy for mechanobiology research and tissue engineering.

1. Introduction

The capability of modulating cell phenotype is important in the design and manufacturing of tissue-engineered scaffolds. Scaffold stiffness significantly affects the intercellular stress conduction chain from the matrix, focal adhesions, and stress fibres to the nucleus, thereby modulating cellular behaviours such as polarisation, migration, and differentiation [1–6]. The commonly used models to research matrix stiffness and cell behaviours are hydrogels [7, 8] or PDMS matrix [9, 10]. However, these matrices often lack the extracellular matrix (ECM)-mimicked topographical features of the native ECM, which limits the ability to replicate a bionic microenvironment for building multi-tissue *in vitro* models to research in-depth interactions.

Electrospinning is a promising technique for fabricating fibrous scaffolds with different topographies for ECM mimicking scaffold fabrication [11–13]. Methods for achieving wide range stiffness are limited, and the commonly used methods such as,

© 2025 The Author(s). Published by IOP Publishing Ltd

changing solution system [14–16] or post-processing [17–19], may compromise topography uniformity and comparability. For example, physical processing such as thermal treatment or chemical processing such as crosslinking can alter not only the stiffness but also the surface roughness, porosity, or chemical composition of the material [14, 15, 18]. These changes are linked with varying cellular responses, making it difficult to attribute specific cell phenotype and behaviour changes to a single factor, such as stiffness.

The fabrication of fibrous matrices through wet-electrospinning is a promising technique, in which, electrospun fibres are deposited into a liquid bath filled with a non-solvent liquid [20–23]. This method, which involves a secondary collection process, allows for tuning physical properties such as fibre diameter while maintaining topographical uniformity [24]. Stiffness modulation, however, has not been explored in wet-electrospinning. This could be attributed to the sub-microscale dimensions, whereby microscale bundles are prone to breakage as they easily exceed the maximum tensile force [25]. Due to this instability, research on the effects of secondary collection behaviours on fibre stiffness adjustment is limited.

In this study, the electrostatic attraction force from a positively charged auxiliary plate electrode can serve as a protective method, preventing stress concentration and creating a stable collection environment across a wide range of collection speeds. This auxiliary setup can be effectively combined with wet-electrospinning during the bundle collection process, as the liquid bath removes the charge on the fibres, rendering them electrostatically neutral, which can then be electrostatically attracted. The study finds that adjusting the collection speed can tune the stiffness of the fibres while maintaining their morphology, enabling the production of stiffness-tunable bundles and facilitating cell polarisation.

2. Materials and methods

2.1. Materials

The polymers used were polycaprolactone (PCL, Mw = 80 000), poly(vinylidene fluoride-co-hexafluoropropylene) (PVDF-co-HFP, Mw = 455 000), polyacrylonitrile (PAN, Mw = 150 000), and poly(vinyl chloride) (PVC, Mn = 47 000). The solvents used were N,N-dimethylformamide (DMF)/chloroform mixture for PCL; DMF/acetone for PVDF-co-HFP; DMF for PAN; and DMF/tetrahydrofuran (THF) for PVC. All polymers and solvents were purchased from Sigma (Merck, UK) and used without further purification. The Dulbecco's Modified Eagle Medium-low glucose (DMEM-L glucose), PrestoBlue reagent, Live/Dead assay kit, were purchased from Thermo Fisher.

2.2. Set-up

An improved wet-electrospinning setup was used in this study, which included a high-voltage generator (0–40 kV, Linari, Italy) for the needle and another high-voltage generator (0–30 kV, Teslaman, China) for the auxiliary plate electrode, a pump (Model 300, WPI, UK), and a modified collector. The modified collector consisted of an earthed stainless steel liquid bath (D = 20 cm) filled with distilled water (DI water). A rotating drum (D = 9 cm, 0–1300 rpm) was mounted on a single-axis reciprocating motion platform to drag the electrospun fibres. An auxiliary plate electrode (2 × 5 × 0.1 cm, aluminium) was used to provide an electrostatic attraction force. The schematic of the setup is shown in figure 1.

Polymer solutions were loaded into a 20 ml PP syringe, transferred via a PTFE tube (ID 1/8 inch), and fitted with a 21 G stainless steel blunt needle, 9 cm from the liquid bath. A 13 kV voltage was applied to the needle, and an 11.5 kV voltage was applied to the auxiliary plate electrode. The grounding electrodes of both high-voltage generators were connected to the liquid bath. The electrospun fibre bundle samples were collected at room temperature with around 55% humidity, dried in a hood overnight, and stored in a vacuum desiccator.

During electrospinning, the positively charged fibres deposited on the surface of the DI water at 25 °C, earthed), forming a neutralised charged fibre mesh, followed by dragging and winding onto a rotating drum. During dragging, the non-woven fibre web received force, causing the fibres to rearrange into an aligned structure. The neutralised charged aligned fibres then received electrostatic attraction from the positively charged auxiliary plate electrode, reducing the total corresponding tensile stress. The electrostatic attraction force provided by the auxiliary plate offset part of the resistance and gravity, greatly reducing the tensile stress and dramatically increasing the collection speed range (figure 1(a)).

The top-down view of the wet-electrospinning setup illustrates the bundle collection process (figure 1(b)). A close-up image of the auxiliary electrode, applying a higher voltage, generated an electrostatic attraction force significantly greater than the gravitational pull on the fibres, resulting in a dramatically deformed trajectory (figure 1(c)).

2.3. Solutions preparation

The polymer solution systems are summarised in table 1. PCL was dissolved in a mixed solvent of DMF/chloroform (2/8 v/v) at a concentration of 13% w/v [26–28]. PVDF-co-HFP was dissolved in a mixed solvent of DMF/acetone (4/6 v/v) at a concentration of 11.5% w/v [29–31]. PAN was dissolved in DMF at a concentration of 8% w/v [32–34]. PVC was dissolved in a mixed solvent of DMF/THF at a concentration of 13% w/v [35, 36]. Those solution systems are commonly used in the wet-electrospinning

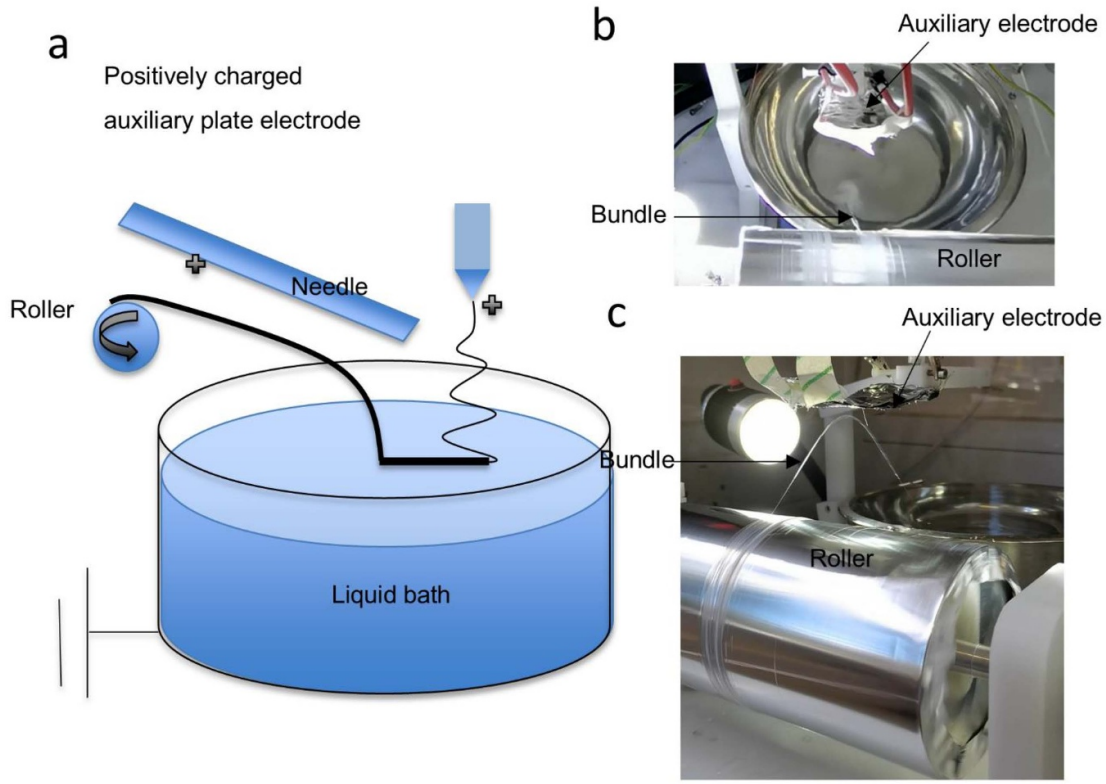

Figure 1. (a) Schematic figure Illustration of the wet-electrospinning setup. (b) Top-down view photograph of the bundle production in progress. (c) Close-up of auxiliary electrode images emphasising the electrostatic attraction force applied by the auxiliary electrode.

Table 1. Summary of polymer solutions.

Polymer	Solvent (v/v)	Concentration (w/v %)	Flow rate (ml/h)
PCL	DMF/Chloroform 2/8	13	1
PVDF-co-HFP	DMF/Acetone 4/6	11.5	1
PAN	DMF	8	1
PVC	DMF/THF 5/5	13	1

study due to the ductility of the materials and their concentrations were adopted from previous wet-electrospinning studies. Homogeneous solutions were prepared by overnight stirring at room temperature to achieve a uniform status.

2.4. Wet-electrospinning of PCL, PVDF-co-HFP, PAN and PVC

The process parameters for electrospinning and fibre bundle fabrication are summarised in table 2. Polymer solutions (table 1) were electrospun into liquid bath at different collection speeds to observe the collection effects on the bundle width and fibre morphology (table 2).

Specifically, 13 w/v% PCL in DMF/Chloroform (2/8, v/v) was used to reveal the effects of voltage applied on auxiliary plate electrode, the working distance between needle and liquid bath and collection speed (set 1, table 2). The applied voltage on auxiliary was varied from 8–12.5 kV (0.5 kV as interval) and working distance between needle and liquid bath was15 cm.

To reveal the mechanism of fibre bundle formation and the relationship between collection speed and fibre bundle width, 13 w/v% PCL in DMF/Chloroform (2/8, v/v), 11.5 w/v% PVDF-co-HFP in DMF/Acetone (4/6, v/v), 8% w/v PAN in DMF and 13% w/v PVC in DMF/THF were collected at various collection speeds (set 4, table 2). To reveal the relationship between collection speed and PCL fibre bundle mechanical properties, 13% w/v PCL in DMF/Chloroform (2/8, v/v) was used to fabricate fibre bundle with around 100 μm thickness at different collection speeds (set 1, table 2).

To evaluate the cell response on wet-electrospun fibre bundle-based scaffold, PCL wet-electrospun fibre bundles collected at different speeds were used for *in vitro* cell culture. PCL electrospun random

Table 2. Summary of wet-electrospun fibre bundle samples and collection parameters.

Solution	Electrospinning parameters (needle voltage /working distance)	Collection parameters (auxiliary electrode voltage/ collection speed)
13% w/v PCL in DMF/chloroform (2/8, v/v)	13 kV/15 cm	8–12.5 kV/ 10–120 m min^{-1}
11.5% w/v PVDF-co-HFP in DMF/acetone (4/6, v/v)	13 kV/15 cm	11.5 kV/13–34 m min^{-1}
8% w/v PAN in DMF	13 kV/15 cm	11.5 kV/13–28 m min^{-1}
13% w/v PVC in DMF/THF (5/5, v/v)	13 kV/15 cm	11.5 kV/18–38 m min^{-1}

and aligned fibre collected from rotation drum at the speed of 60 rpm and 1000 rpm were selected (figure 1(b)). The samples were ∼100 μm thick and punched into discs (diameter = 10 mm). All samples were stored in a vacuum desiccator for 14 d to remove retained solvents before testing.

2.5. Simulation

A 2D stationary study was conducted using the 'Electrostatics' and 'Solid Mechanics' modules in COMSOL Multiphysics® 6.2 (COMSOL AB, Sweden) to investigate the effect of changing secondary electrode voltage on the electrostatic field and its application in facilitating bundle collection.

The geometry setup replicated the experimental conditions, with the bundle fixed at both ends, connected to a rotary collector and a liquid bath surface. Material properties were based on a bundle fabricated at 50 m min^{-1} using this setup. A sufficiently large resolution domain filled with air was used to compute the electrostatic field. The liquid bath was earthed at the bottom, and the drum was set as the floating potential to simulate a hollow rotating drum. The electric field was applied using the Electrostatics module at two voltage levels: 0 kV and 11.5 kV on the secondary electrode, and 13 kV on the primary electrode.

The model applied both gravity and electrostatic forces, assuming all geometric entities were homogeneous in properties. Uniform potential was set on the electrode boundaries without considering the electric field distribution within the electrodes. Gravitational force was applied to the yarn samples, and the coupling between electrostatic and mechanical forces was handled using the built-in 'Electromechanical Force' node. The mesh was automatically generated using the 'extra fine' setting. The stress and strain results for the bundle were presented in a colour map.

2.6. Characterisation

Optical microscopy (Axioskop 2 Plus, Zeiss, UK) was used to measure the fibre bundle width and observe wet-electrospun random fibres, wet-electrospun bundle morphology and width under the 200× magnificent. The determination of fibre morphology, fibre bundle width, via optical microscopy imaging, was performed by the collection of fibres or bundles on a slide mounted on the collector (liquid bath surface/rotation drum) at the beginning of the process.

Further, scanning electron microscopy (SEM; Phenom ProX, USA) was applied with a 5 kV acceleration voltage to study wet-electrospun fibre and bundle morphology and diameter. Carbon tape was attached on collectors to capture samples (figure 2). Gold coating enables samples to be electrically conductive. ImageJ 1.8.0 (NIH, USA) was employed to analyse the fibre bundle width ($n = 6$) from optical microscope images and topography and fibre diameter distribution (random selection of 100 nanofibres) from SEM images.

Tensile test was performed to research the effects of collection speed on PCL fibre bundle mechanical properties, compared with random and aligned electrospun samples ($n = 11$). The PCL electrospun fibre bundle, random and aligned samples were cut into 30 × 10× 0.1 mm samples. Tensile test performed on the Zwick 005 machine (Germany), with a 20 mm initial gap-to-gap separation, 15 kPa pre-loaded stress, 50 mm min^{-1} test speed, to record the stress-strain curve.

Sample porosity was indirectly measured via apparent density method. wet-electrospun PCL fibre bundle and electrospun random and aligned PCL fibre ($n = 5$) were cut 10*10*0.1 mm. The volume was calculated via measuring thickness, width and length of samples. The thickness was measured via thickness (1 μm) gauge. The weight was measured via microbalance (Mettler Toledo, UK).

To identify the effects of collection speed on crystalline changes, wet-electrospun PCL bundles collected at 0, 50, and 110 m min^{-1} were tested via x-ray diffraction (XRD) (Rigaku, MiniFlex 600). The tests were performed using CuKα radiation at a scanning rate of 2°min^{-1} (2θ), with an operating voltage of 40 kV and a current of 15 mA, over a range of 10°–40°. Local software was used to automatically process the data.

2.7. *In vitro* evaluation

Sheep bone marrow mesenchymal stem cells (BMMSCs) were evaluated on fibre bundle scaffolds.

Cell culture was described in previous work [37, 38]. In brief, BMMSCs were cultured in flasks at 37 °C and 5% CO_2 in a humidified atmosphere. The cell culture medium was Dulbecco's modified Eagles' medium (DMEM, Sigma, Merk, UK), added with 10% fetal calf serum (FCS, First Link, UK), 1% penicillin and streptomycin (P/S, Gibco, UK). 80% confluence was regarded as the necessity of cell passage. Cells at passages 5–15 were used

Wet-electrospun PCL fibre bundles ($n = 5$) were evaluated for cell proliferation, viability (Live/Dead assay), and morphology (SEM). The samples were cut into 10 mm diameter discs and sterilised in 70% ethanol overnight. After three washes with phosphate-buffered saline (PBS; 5 min each), the samples were pre-conditioned in low-glucose DMEM overnight. The discs were then transferred into 48-well plates. A 20 μL cell suspension containing 30 000 cells was seeded onto each pre-wetted scaffold. After 4 h of incubation, 400 μL of complete cell culture medium was added to each well.

PrestoBlue was used to assess cell proliferation on days 1, 3, and 7, following the supplier's protocol. Briefly, before each measurement, the samples were transferred to a fresh 48-well plate. A mixture of 400 μL of culture medium and PrestoBlue (9:1, v/v) was added to each well, followed by incubation for 1 h. Absorbance was measured at 570 nm with 600 nm as a reference wavelength. Cell numbers were estimated using a standard calibration curve. For viability staining, 4 μM ethidium homodimer and 2 μM calcein AM were added to each well, followed by incubation for 30 min at room temperature in the dark. Fluorescence microscopy was used to capture images of viable and non-viable cells. To assess cell morphology, samples from days 1 and 7 were fixed in 2.5% (v/v) glutaraldehyde and dehydrated in a graded ethanol series. Final dehydration was performed using hexamethyldisilazane for 5 min, followed by air drying overnight. The SEM imaging parameters were the same as previously described.

2.8. Statistical analysis

All results are presented as mean ± standard deviation. Statistical analyses and plotting were conducted using Origin software. For comparisons involving the fibre diameter, an independent T-test was used to determine the significance of differences between two groups. For cell proliferation experiments, two-way analysis of variance was used to analyse the significance level of differences between timepoints and groups, and post-hoc comparisons were performed using the Tukey's honest significant difference test, with results displayed as P-values, where *, **, and *** correspond to $P < 0.05$, $P < 0.01$, and $P < 0.001$, respectively.

3. Results

3.1. Wet-electrospun PCL fibres and bundles

3.1.1. Experimental

The experimental results of PCL bundle collection demonstrated that the voltage applied to the auxiliary plate electrode significantly increased the maximum collection speed. A series of tests gradually increasing the auxiliary voltage from 0 to 13 kV were conducted to determine the optimal condition (figure 2(a)). When the voltage exceeded 11.5 kV, the excessive electrostatic force disrupted fibre alignment and hindered continuous collection. The highest stable collection speed was achieved at 11.5 kV, allowing continuous bundle formation at 120 m min^{-1}. This indicates that at 11.5 kV, the electrostatic assistance effectively counterbalanced gravitational sagging and minimised stress accumulation at the bundle ends, promoting a more stable collection process. This change in collection speed was attributed to the electrostatic force applied to the bundle. In the initial stage+, as the voltage increased, the electrostatic force strengthened, offsetting gravity. However, beyond the optimal range, the overwhelming electrostatic force destabilised the bundle trajectory (figure 1(c)). Therefore, 11.5 kV was selected as the optimised voltage for the following experiments. Subsequent simulation analysis further confirmed the stress distribution regulation under the auxiliary electrode condition.

A decrease in the fibre bundle width was observed (figure 2(b)). The width of the PCL fibre bundle was 344.63 ± 50.07 μm at 10 m min^{-1} collection speed, reaching a plateau at 50 m min^{-1} (59.60 ± 10.30 μm), and showing an ultra-fine fibre bundle at 100 m min^{-1} collection speed (30.29 ± 5.36 μm).

Fibre diameter reduction was observed within the fibres collected at 0, 20, 50, 80, and 110 m min^{-1}. Other features such as morphology retention and single-layer aligned fibre bundles were noted as well (figure 2(c)). In PCL wet-electrospun random samples, micro sized fibres (1.42 ± 0.42 μm) with rough surfaces featuring surface pores. These features were consistently observed in SEM images across all bundle samples. The holes in PCL samples are expected to form due to water droplet condensation on the fibres, resulting from the rapid endothermic solvent volatilisation. Additionally, fibre loops were observed in the structure. The fibre diameter of PCL electrospun random fibres was significantly thicker (1.80 ± 0.30 μm) than those collected via wet-electrospinning. The fibre diameter decreased with the increase in collection speed, reaching 1.02 ± 0.27 μm at the highest speed (figure 2(d)). This trend is likely due to the stretching force exerted on the fibres during collection.

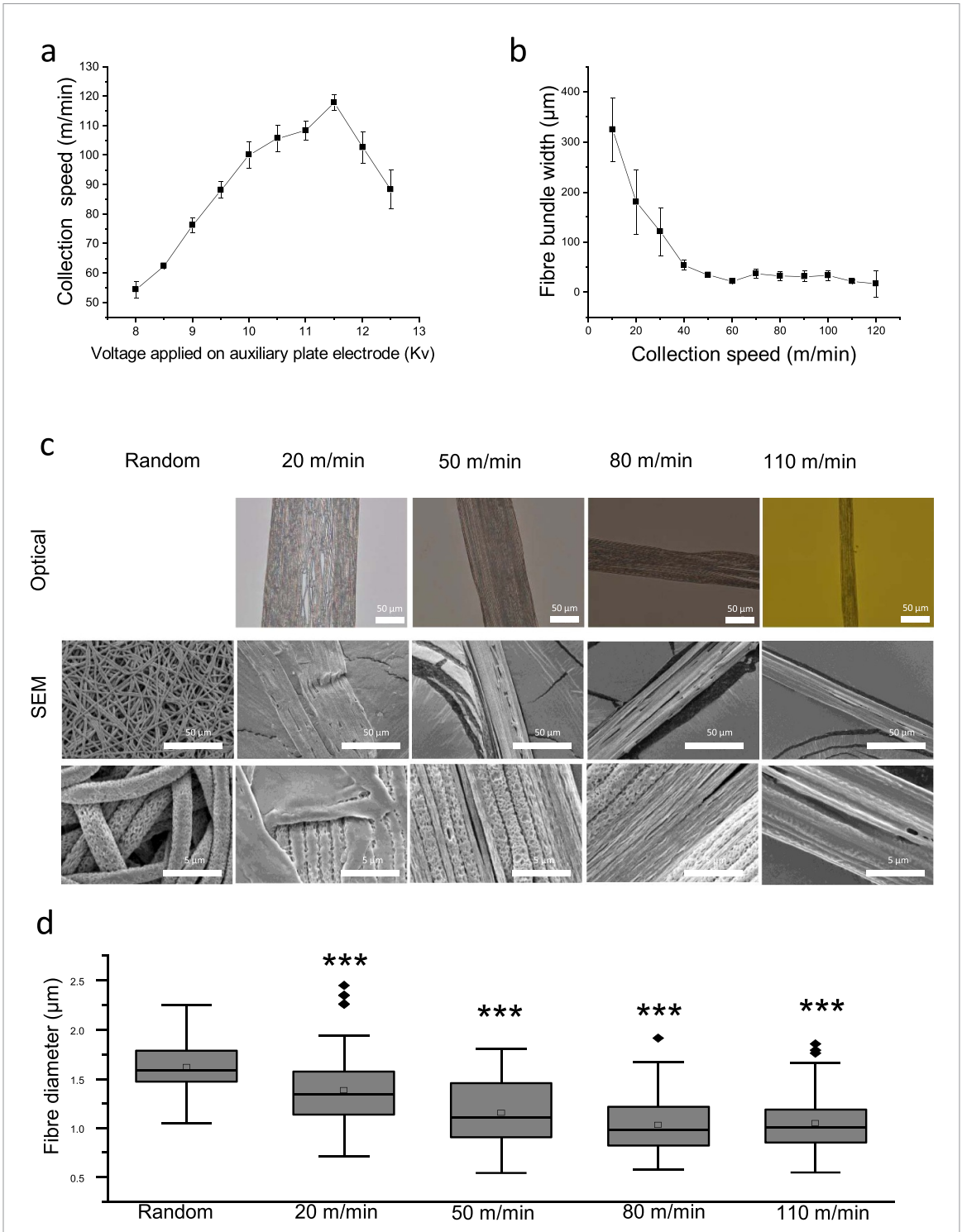

Figure 2. Wet-electrospun PCL bundle collection under various parameter settings. (a) The effect of voltage applied on auxiliary plate electrode and collectors on continuous collection speed. (b) The effect of collection speed and fibre bundle width of PCL. (c) Influence of collection speed on the morphology of fibre bundles. SEM images captured at high and low magnification show the fibre bundles collected at speeds of 0, 20, 50, 80, and 110 m min^{-1}. (d) The fibre diameters were statistically analysed, and the results were compared with those at 0 m min^{-1}. Significant differences are indicated by asterisks: * for $p < 0.05$, and *** for $p < 0.001$.

3.1.2. Simulation

The effect of the secondary electrode on fibre bundle collection was investigated using a coupled Electrostatics and Solid Mechanics model in COMSOL Multiphysics. Simulations were conducted under two conditions by applying 0 kV and 11.5 kV to the secondary electrode to assess the electrostatic influence (figure 3(a)). The results indicated that applying voltage to the secondary electrode significantly enhanced the electric field strength in the vicinity of the yarn, thereby increasing the electrostatic force during the collection process.

In the absence of voltage on the secondary electrode, the yarn was primarily affected by gravity

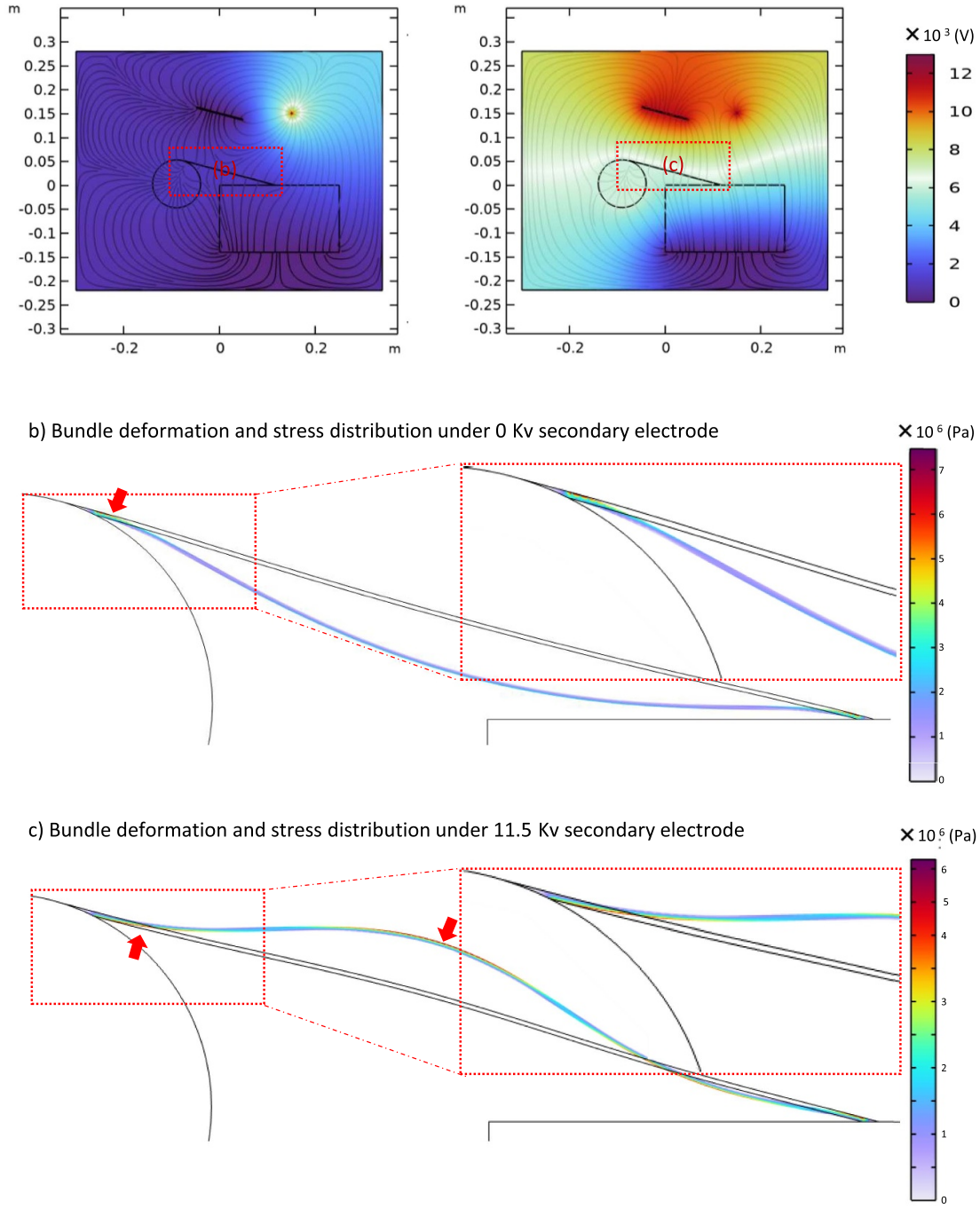

Figure 3. The summary of simulation results. (a) Electric field distribution patterns at 0 kV (left) and 11.5 kV (right) applied on the secondary electrode. Deformation and stress distribution of the bundle under the influence of gravity and electrostatic force from a (b) 0 kV or (c) 11.5 kV secondary electrode. The left panel shows the deformation pattern of the yarn, indicating the overall displacement due to the combined forces. The enlarged view of the stress concentration areas within the yarn.

(figure 3(b)), resulting in a characteristic catenary shape with stress concentrated at both the rotating drum end and the water surface exit point. In contrast, when voltage was applied, the yarn experienced upward electrostatic forces that counteracted gravity, reducing stress at both ends and distributing it more uniformly along the yarn (figure 3(c), as indicated by red arrows).

3.2. Validation of wet-electrospun bundle fabrication system versatility with other materials

The same bundle-forming characteristics were also observed in wet-electrospun fibres and bundles fabricated from 11.5%w/v PVDF-co-HFP, 8%w/v PAN, and 13%w/v PVC (figure 4). For all materials, fibre bundle width decreased with increasing collection speed. In PVDF-co-HFP bundles, the width

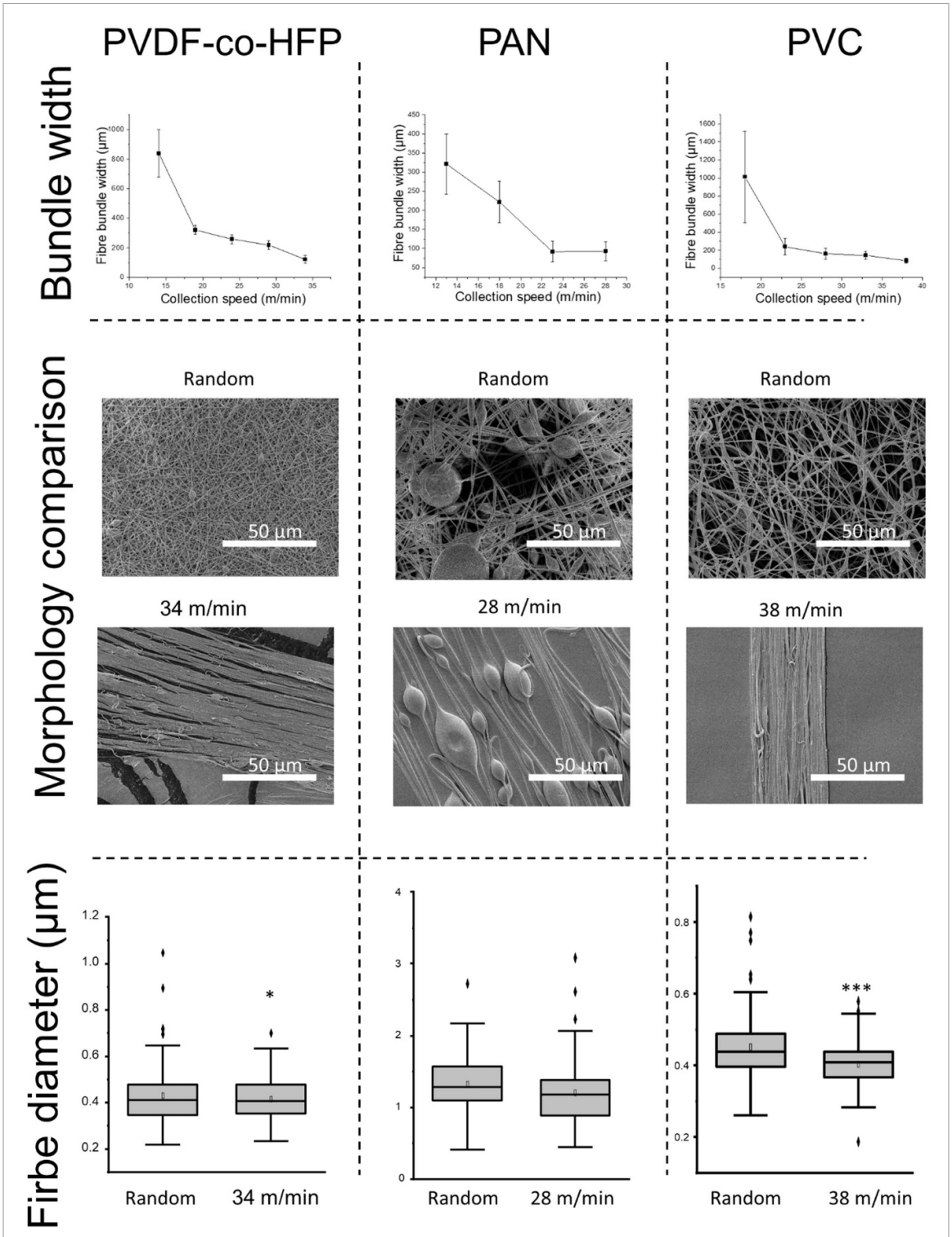

Figure 4. Evaluation of System Versatility Using Different Materials. PVDF-co-HFP, PAN, and PVC were evaluated. Bundle width, bundle morphology, and fibre diameter were assessed. The 'ns' and '***' mean $P > 0.05$ and $P < 0.005$ respectively. ($n = 100$).

reduced from 1012.50 ± 507.68 μm at 18 m min^{-1}–82.47 ± 30.00 μm at 38 m min^{-1}. In PAN bundles, the width decreased from 321.15 ± 78.82 μm at 13 m min^{-1}–93.46 ± 24.74 μm at 28 m min^{-1}. A significant reduction was also observed in PVC bundles, from 839.32 ± 161.30 μm to 120.89 ± 27.95 μm at 18 m min^{-1} and 38 m min^{-1}, respectively.

Fibre morphology remained consistent across all materials, maintaining a single-layer aligned structure. Loop-like structures were also present, likely resulting from fibre bending during the collection process. A reduction in fibre diameter with increasing collection speed was also observed in all groups.

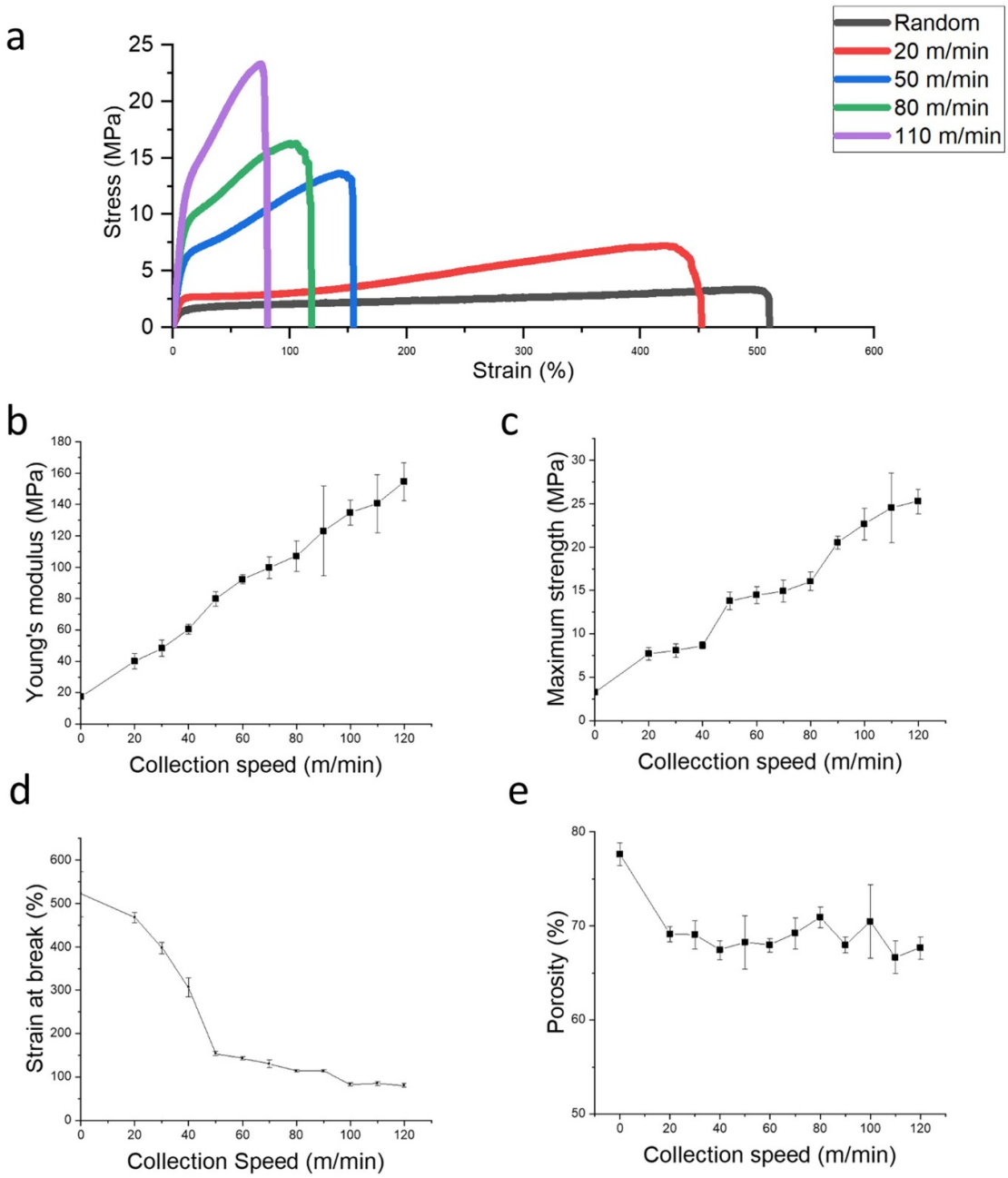

Figure 5. The effect of collection speed on the mechanical properties and porosity of wet-electrospun PCL bundles. The figure includes: (a) a typical stress and strain curve, (b) Young's modulus, (c) maximum strength, (d) strain at break, and (e) porosity.

3.3. Collection speed modulating PCL bundle strength

Tensile tests were performed on PCL electrospun random fibres, aligned fibres, and wet-electrospun bundles collected at different speeds ($n = 10$) to investigate the effects of fabrication method and collection speed on mechanical properties, including Young's modulus, maximum tensile strength, and strain at break. Figure 5 shows representative stress–strain curves for each sample. Random fibres exhibited a Young's modulus of 17.42 ± 1.01 MPa (figure 5(b)), a maximum tensile strength of 3.26 ± 0.33 MPa (figure 5(c)), and (a) strain at break of 522.59 ± 52.74% (figure 5(d)). In comparison, wet-electrospun PCL bundles showed significantly enhanced mechanical properties. As the collection speed increased, both Young's modulus and maximum tensile strength improved, while strain at break decreased. Specifically, the Young's modulus increased from 39.98 ± 4.89 MPa at 20 m min^{-1}–107.26 ± 9.68 MPa at 80 m min^{-1}. The corresponding maximum tensile strength rose from 7.69 ± 0.72 MPa to 16.06 ± 1.07 MPa. In contrast, the strain at break decreased from 468.45 ± 13.01%

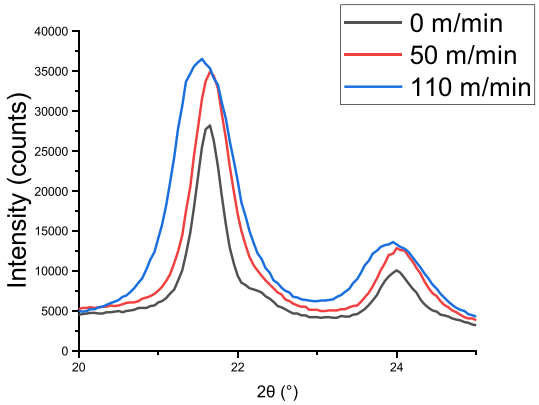

Figure 6. XRD data of wet-electrospun PCL bundle collected at various speeds.

Table 3. Summary of peaks results at 21.5° and 24°.

		Height (cps)	FWHM (deg)	Int. I (cps deg)	Size(ang.)
21.5 °	Control	11 263.42	0.4057	7533.02	208.22
	50 m min^{-1}	14 401.27	0.5393	12 285.32	156.65
	110 m min^{-1}	15 602.89	0.867	19 312.79	97.42
24 °	Control	2876.34	0.5812	2230.05	145.94
	50 m min^{-1}	3923.08	0.7058	3349.9	120.18
	110 m min^{-1}	4702.84	0.9885	6655.26	85.8

to 114.51 ± 2.67%. Notably, even bundles collected at 80 and 110 m min^{-1} retained sufficient elongation to meet the mechanical flexibility requirements for soft scaffold applications.

The porosity of the samples ($n = 5$) was determined using a gravimetric method (figure 5(e)). All wet-electrospun samples exhibited high porosity values, with a minimum of 66.04 ± 2.02%. The PCL random fibres demonstrated the highest porosity at 77.65 ± 1.65%, which was significantly greater than that of fibres collected from the liquid bath surface. The porosity of fibre bundles collected at different speeds ranged from 66.04% to 73.85%, with no statistically significant differences. This suggests that the observed variations in mechanical properties were not primarily influenced by differences in porosity.

XRD analysis revealed that increasing the collection speed resulted in reduced grain size and increased crystallinity (figure 6). Specifically, at $2\theta = 21.5°$, the crystal size decreased from 208.22 Å in the control group to 97.42 Å at 110 m min^{-1}, while at $2\theta = 24°$, it decreased from 145.94 Å to 85.8 Å table (3). Concurrently, the full width at half maximum (FWHM) values increased with collection speed, indicating a broadening of diffraction peaks. This trend suggests the refinement and partial crystal disintegration. Overall, higher collection speeds led to smaller grain sizes and more dispersed crystal structures.

3.4. *In vitro* evaluation

Figure 7 shows the cell number on each sample at days 1, 3, and 7. An increasing trend in cell number was observed across all groups, indicating that wet-electrospun PCL bundles support cell proliferation. At all time points, no statistically significant differences were found between bundles fabricated at different collection speeds, suggesting that collection speed had a limited effect on surface topography or the resulting cell microenvironment.

SEM was used to examine cell morphology and the cell–material interface (figure 8). Enhanced cell proliferation was observed from day 1 (D1) to day 7 (D7). On D1, cells adhered to all samples, as evidenced by the extension of filopodia. However, cells on D1 appeared smaller and more rounded compared to those on D7. After 7 d, cells showed greater spreading, with spindle-shaped morphologies aligned along the fibre direction. This alignment was observed on all samples except the wet-electrospun bundle collected at 20 m min^{-1}, suggesting that fibre orientation may guide cell elongation and alignment.

To further evaluate cell viability and distribution, Live/Dead staining was performed on days 1 and 7. Viable cells were stained green, while dead cells were stained red. The results were consistent with both proliferation and SEM findings, demonstrating cell survival and expansion on all samples. On D1, a limited number of viable cells and a

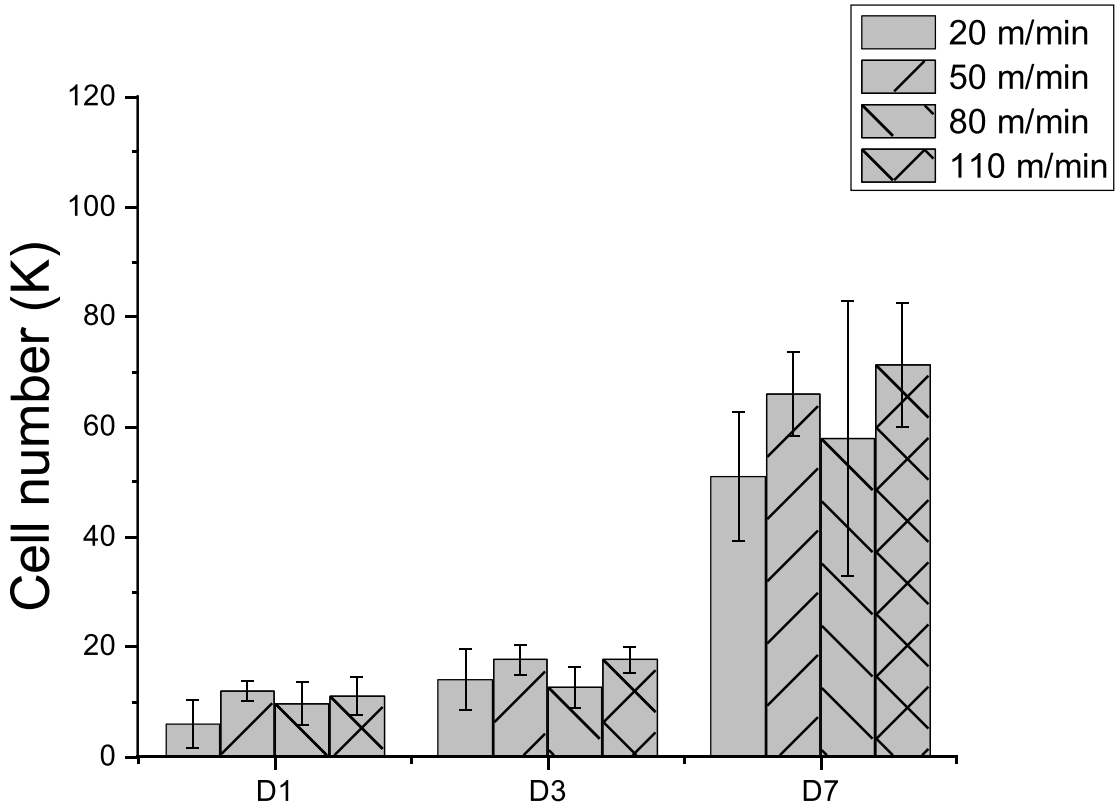

Figure 7. Cell number wet-electrospun fibre bundle fabricated under the 20. 50. 80, 100 m min^{-1} collection speed, at 1, 3, 7 d of culture. No significant difference was observed.($n = 5$).

few dead cells were observed. The initial cell density on wet-electrospun bundles was lower than that on random electrospun fibres. By D7, live cells had reached confluence on the random electrospun samples and covered most of the surface area of the wet-electrospun fibre bundles.

4. Discussion

This work introduces an electrostatic-assisted wet-electrospinning setup, enabling scaffold stiffness modulation and controlling cell polarisation. Understanding how mechanical modulation via collection speed affects scaffold stiffness and the following cellular responses is the focus. Although wet-electrospinning has been used to fabricate bundles, its effect on fibre properties and mechanotransduction remains poorly understood. This section will discuss set-up improvements, mechanical tuning mechanisms, and explore implications for cellular behaviour, as well as the limitations.

In terms of wet-electrospinning setups, the benchmark was established by Smit *et al* [23], primarily focusing on bundle formation through floating collection. Since then, various parameters have been investigated to optimise bundle morphology, including bath liquid selection, bath temperature adjustment, and the introduction of accessories to modulate surface patterns, bundle diameter, and twisting configurations. However, electrofield, this intrinsic property, was overlooked in the dynamic wet-electrospinning process, where the fibre bundle is collected from a liquid bath to a rotary drum. Our research revealed that the electrofield not only plays a vital role in electrospun fibre deposition [39, 40], but also acts as a key factor during the secondary fibre collection process.

The successful role of the secondary electrode relies on the liquid bath, which removes the charge from the deposited fibre and maintains fibre mobility. The mobility of the deposited fibre in the bath liquid allows the use of a secondary collector, such as a drum, to draw the fibre from the liquid bath to the drum. The removal of the charge neutralises the fibre, enabling it to be attracted by the secondary high voltage via electrostatic force and, therefore, enabling high-speed collection.

The stiffness change was attributed to the tension from high-speed collection, which affects the PCL bundle crystal structure. According to previous AFM studies, electrospun PCL fibre consists of lamellar crystal stacks perpendicular to the fibre axis, connected by amorphous ties [41, 42]. The application of tensile force aligns the amorphous PCL chains, breaking the large crystals into smaller ordered structures to increase stiffness [43]. In this study, as the collection speed increased, fibres were subjected to higher extensional forces during alignment and winding,

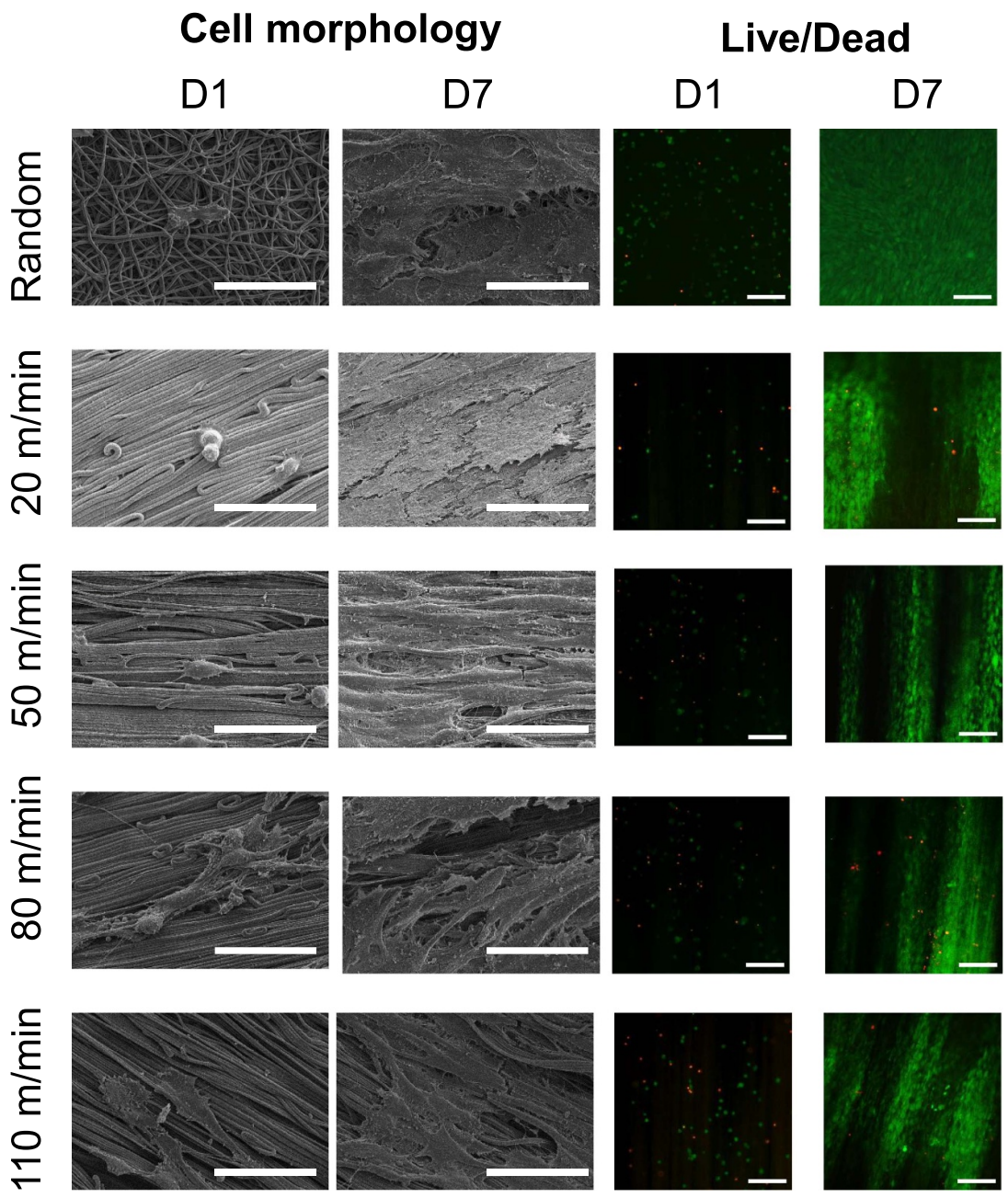

Figure 8. SEM images of cells seeded on wet-electrospun fibres and bundles fabricated under the 20, 50, 80, and 100 m min^{-1} collection speeds, at 1 and 7 d of culture. Live/Dead (green/red) images of cells seeded on electrospun random/aligned fibres and wet-electrospun fibre bundles fabricated under the 20, 50, 80, and 100 m min^{-1} collection speeds, at 1 and 7 d of culture. Scale bar = 200 μm.

which may fragment lamellar structures into smaller crystalline domains. A significant reduction in crystal size was measured, with crystal size decreasing from 208 Å when collected at 0 m min^{-1} to 97 Å when collected at 110 m min^{-1} [43]. This value was smaller than that reported by Jordan and Korley [43], where during tensile testing of PCL fibres, the crystal size measured at the (110) plane was reduced from 400Å initially to around 150Å after 60% strain and then stabilised. This difference may be due to approximately 1% to 15% [44, 45] residual solvent in the as-spun fibres, which may cause the crystals between fibres to slip or disintegrate more easily. Together, these effects explain the observed modulus enhancement across the collection speed gradient.

Compared with current stiffness modulation methods, this approach maintains consistent topography and does not introduce additional chemical components. The topographic consistency was attributed to selecting deionised water as the bath liquid, refining fibres into a single-layer bundle structure. Specifically, water with high surface tension kept the deposited electrospun fibre floating on the surface, maintaining a parallel arrangement from deposition

to rearrangement and drawing from the bath liquid to the air. Also, this method does not introduce additional chemicals, as the DI water evaporates after collection.

Cellular polarisation modulation is another highlight of this scaffold. High-stiffness matrices support cytoskeletal organisation through mechanosensing, promoting the formation of aligned actin filaments and nuclear elongation, which benefits tendon and ligament scaffold development due to its influence on cell phenotype [46–48]. A high-stiffness matrix constrains cell contraction and therefore maintains high intercellular stress, promoting aligned actin network formation. Interestingly, cells lost their spindle shape to some degree at higher stiffness, such as in fibres collected at 110 m min^{-1}, a phenomenon that has been reported with limited mechanistic explanation [49–52]. A recent study by Doss *et al* [53] suggests that overexpression of actin arising from a high-stiffness matrix requires an even higher matrix stiffness. If the increase in material stiffness cannot match the increase in cell stiffness, cell polarisation disappears.

Despite demonstrating scaffold stiffness modulation and preliminary control of cell morphology, several limitations should be acknowledged. First, this study primarily focused on mechanical characterisation, while detailed biological responses such as cell behaviours, gene expression, and cytoskeletal changes were not investigated. The intracellular structure should be stained to further refine the fibre–cell interaction. The bundle matrix would benefit from additional AFM-based mechanical mapping. Future work will focus on cell behaviours to elucidate the broader impact of scaffold stiffness on cellular function.

Together, these findings highlight the potential of electrostatic-assisted wet-electrospinning for controlled mechanical tuning of fibre bundles and scaffold-based mechanobiological studies, warranting further exploration in future research.

5. Conclusion

In this study, we developed a wet-electrospinning system integrated with a positively charged auxiliary electrode, enabling scaffold stiffness modulation while preserving topographical consistency, ultimately leading to controlled modulation of cell morphology. This tunable stiffness was achieved via high-speed collection, during which the applied tensile stress induced crystal disintegration and refinement within the PCL bundles. The smooth and continuous collection process was facilitated by the auxiliary electrode, which provided electrostatic force to reduce stress concentration at the bundle ends. As a result, a desirable tunable stiffness range from 40 MPa to 120 MPa was achieved and effectively used to modulate cell phenotype. Unlike conventional approaches that alter topographical cues or require changes in chemical composition to tune stiffness, this method maintains topographical comparability. This electrostatic-assisted collection strategy provides a reliable platform for fabricating stiffness-tunable scaffolds, supporting investigations in musculoskeletal tissue engineering and mechanotransduction models.

Data availability statement

All data that support the findings of this study are included within the article (and any supplementary files).

Acknowledgment

This work was supported by the Engineering and Physical Sciences Research Council via the DTP CASE Programme [Grant Number EP/T517793/1], the NIHR UCLH BRC- UCL Therapeutic Acceleration Support (TAS) Fund [Grant Number 564021—linked to Lead 557 595], and the European Commission via H2020 iP-OSTEO programme (Project No. 824007).

Compliance with ethics guidelines

All authors declare that they have no conflict of interest.

This study does not contain any studies with human or animal subjects performed by any of the authors.

Author contributions

Haoyu Wang 0000-0002-3513-7037
Conceptualization (equal), Data curation (equal), Formal analysis (equal), Investigation (equal), Methodology (equal), Software (equal), Visualization (equal), Writing – original draft (equal), Writing – review & editing (equal)

Chelsea Violita Stanley
Data curation (equal), Visualization (equal), Writing – original draft (equal), Writing – review & editing (equal)

Xiangshen Gao
Formal analysis (equal), Software (equal), Writing – original draft (equal), Writing – review & editing (equal)

Ziyu Liu
Formal analysis (equal), Visualization (equal), Writing – original draft (equal), Writing – review & editing (equal)

Mo Zhou 0009-0001-8776-8543
Formal analysis (equal), Validation (equal), Visualization (equal), Writing – original draft (equal), Writing – review & editing (equal)

Mingjing Zhang
Formal analysis (equal), Visualization (equal), Writing – original draft (equal), Writing – review & editing (equal)

Feng-lei Zhou 0000-0002-8348-4658
Supervision (equal), Visualization (equal), Writing – original draft (equal), Writing – review & editing (equal)

Maryam Tamaddom
Supervision (equal), Visualization (equal), Writing – original draft (equal), Writing – review & editing (equal)

Chaozong Liu 0000-0002-9854-4043
Conceptualization (equal), Funding acquisition (equal), Project administration (equal), Resources (equal), Supervision (equal), Validation (equal), Visualization (equal), Writing – original draft (equal), Writing – review & editing (equal)

References

[1] Riveline D, Zamir E, Balaban N Q, Schwarz U S, Ishizaki T, Narumiya S, Kam Z, Geiger B and Bershadsky A D 2001 Focal contacts as mechanosensors: externally applied local mechanical force induces growth of focal contacts by an mDia1-dependent and ROCK-independent mechanism *J. Cell Biol.* **153** 1175–86
[2] Gultian K A, Gandhi R, Sarin K, Sladkova-Faure M, Zimmer M, de Peppo G M and Vega S L 2022 Human induced mesenchymal stem cells display increased sensitivity to matrix stiffness *Sci. Rep.* **12** 8483
[3] Song K H, Heo S-J, Peredo A P, Davidson M D, Mauck R L and Burdick J A 2020 Influence of fiber stiffness on meniscal cell migration into dense fibrous networks *Adv. Healthc. Mater.* **9** 1901228
[4] Hiraki H L *et al* 2023 Fiber density and matrix stiffness modulate distinct cell migration modes in a 3D stroma mimetic composite hydrogel *Acta Biomater.* **163** 378–91
[5] Wang R, Thayer P, Goldstein A and Wagner W D 2020 Interaction of material stiffness and negative pressure to enhance differentiation of bone marrow-derived stem cells and osteoblast proliferation *J. Tissue Eng. Regen. Med.* **14** 295–305
[6] Li X, Xu R, Tu X, Janairo R R R, Kwong G, Wang D, Zhu Y and Li S 2020 Differentiation of neural crest stem cells in response to matrix stiffness and TGF-β1 in vascular regeneration *Stem Cells Dev.* **29** 249–56
[7] Li Y, Zhang Y, Shi F, Tao L, Wei Y and Wang X 2017 Modulus-regulated 3D-cell proliferation in an injectable self-healing hydrogel *Colloids Surf. B* **149** 168–73
[8] Lantoine J *et al* 2016 Matrix stiffness modulates formation and activity of neuronal networks of controlled architectures *Biomaterials* **89** 14–24
[9] Swiatlowska P *et al* 2022 Pressure and stiffness sensing together regulate vascular smooth muscle cell phenotype switching *Sci. Adv.* **8** eabm3471
[10] Pandey P *et al* 2018 Cardiomyocytes sense matrix rigidity through a combination of muscle and non-muscle myosin contractions *Dev. Cell* **44** 326–336.e3
[11] Zhang K, Wang X, Jing D, Yang Y and Zhu M 2009 Bionic electrospun ultrafine fibrous poly (L-lactic acid) scaffolds with a multi-scale structure *Biomed. Mater.* **4** 035004
[12] Jin Q, Fu Y, Zhang G, Xu L, Jin G, Tang L, Ju J, Zhao W and Hou R 2022 Nanofiber electrospinning combined with rotary bioprinting for fabricating small-diameter vessels with endothelium and smooth muscle *Composites B* **234** 109691
[13] Li Y, Wang J, Qian D, Chen L, Mo X, Wang L, Wang Y and Cui W 2021 Electrospun fibrous sponge via short fiber for mimicking 3D ECM *J. Nanobiotechnol.* **19** 131
[14] Veleirinho B, Rei M F and Lopes-DA-Silva J 2008 Solvent and concentration effects on the properties of electrospun poly (ethylene terephthalate) nanofiber mats *J. Polym. Sci. B* **46** 460–71
[15] Huang Z-M, Zhang Y Z, Ramakrishna S and Lim C T 2004 Electrospinning and mechanical characterization of gelatin nanofibers *Polymer* **45** 5361–8
[16] Jahanmard F, Baghban Eslaminejad M, Amani-Tehran M, Zarei F, Rezaei N, Croes M and Amin Yavari S 2020 Incorporation of F-MWCNTs into electrospun nanofibers regulates osteogenesis through stiffness and nanotopography *Mater. Sci. Eng. C* **106** 110163
[17] Tan E P and Lim C 2006 Effects of annealing on the structural and mechanical properties of electrospun polymeric nanofibres *Nanotechnology* **17** 2649
[18] Campiglio C E, Ponzini S, De Stefano P, Ortoleva G, Vignati L and Draghi L 2020 Cross-linking optimization for electrospun gelatin: challenge of preserving fiber topography *Polymers* **12** 2472
[19] Zhang T, Lin S, Shao X, Zhang Q, Xue C, Zhang S, Lin Y, Zhu B and Cai X 2017 Effect of matrix stiffness on osteoblast functionalization *Cell Prolif.* **50** e12338
[20] Mejía Suaza M L, Hurtado Henao Y and Moncada Acevedo M E 2022 Wet electrospinning and its applications: a review *TecnoLógicas* **25** e2223
[21] Kostakova E, Seps M, Pokorny P and Lukas D 2014 Study of polycaprolactone wet electrospinning process *Express Polym. Lett.* **8** 554–64
[22] Yokoyama Y, Hattori S, Yoshikawa C, Yasuda Y, Koyama H, Takato T and Kobayashi H 2009 Novel wet electrospinning system for fabrication of spongiform nanofiber 3-dimensional fabric *Mater. Lett.* **63** 754–6
[23] Smit E, Bűttner U and Sanderson R D 2005 Continuous yarns from electrospun fibers *Polymer* **46** 2419–23
[24] Liu J, Liu Q, Ma S, Liang J, Ma X and Fong H 2013 Continuous bundles of aligned electrospun polyacrylonitrile copolymer nanofibers prepared via the flowing water bath and their morphological, structural, and componential variations during the opposite-directional diffusion process *Polymer* **54** 4987–96
[25] Teo W-E, Gopal R, Ramaseshan R, Fujihara K and Ramakrishna S 2007 A dynamic liquid support system for continuous electrospun yarn fabrication *Polymer* **48** 3400–5

[26] Zhou F-L, Hubbard P L, Eichhorn S J and Parker G J M 2012 Coaxially electrospun axon-mimicking fibers for diffusion magnetic resonance imaging *ACS Appl. Mater. Interfaces* **4** 6311–6
[27] Zhang Z, Smith L, Li W, Jiang L, Zhou F, Davies G-L and Williams G R 2022 Polydopamine-coated nanocomposite theranostic implants for localized chemotherapy and MRI imaging *Int. J. Pharm.* **615** 121493
[28] Zhou F-L, Hubbard P L, Eichhorn S J and Parker G J M 2011 Jet deposition in near-field electrospinning of patterned polycaprolactone and sugar-polycaprolactone core–shell fibres *Polymer* **52** 3603–10
[29] Filip P, Zelenkova J and Peer P 2021 Electrospinning of a copolymer PVDF-co-HFP solved in DMF/acetone: explicit relations among viscosity, polymer concentration, DMF/acetone ratio and mean nanofiber diameter *Polymers* **13** 3418
[30] Pyo M, Lee K H and Lee E-J 2024 Enhancing hydrophobicity through polydimethylsiloxane-blended poly (vinylidene fluoride-co-hexafluoropropylene) electrospun membranes: a well-designed approach *Polymer* **307** 127261
[31] Zhou R, Liu W, Kong J, Zhou D, Ding G, Leong Y W, Pallathadka P K and Lu X 2014 Chemically cross-linked ultrathin electrospun poly (vinylidene fluoride-co-hexafluoropropylene) nanofibrous mats as ionic liquid host in electrochromic devices *Polymer* **55** 1520–6
[32] Gomes D S, Silva A N R D, Morimoto N I, Mendes L T F, Furlan R and Ramos I 2007 Characterization of an electrospinning process using different PAN/DMF concentrations *Polímeros* **17** 206–11
[33] Prahsarn C, Klinsukhon W and Roungpaisan N 2011 Electrospinning of PAN/DMF/H_2O containing TiO_2 and photocatalytic activity of their webs *Mater. Lett.* **65** 2498–501
[34] Yu H, Guo J, Zhu S, Li Y, Zhang Q and Zhu M 2012 Preparation of continuous alumina nanofibers via electrospinning of PAN/DMF solution *Mater. Lett.* **74** 247–9
[35] Lee K H, Kim H Y, La Y M, Lee D R and Sung N H 2002 Influence of a mixing solvent with tetrahydrofuran and N, N-dimethylformamide on electrospun poly (vinyl chloride) nonwoven mats *J. Polym. Sci. B* **40** 2259–68
[36] Phatcharasit K, Taweepreda W, Boonkerd K and Kim J K 2013 Preparation and properties of electrospun PVC nanofiber *Adv. Mater. Res.* **770** 193–6
[37] Tamaddon M *et al* 2022 *In vivo* evaluation of additively manufactured multi-layered scaffold for the repair of large osteochondral defects *Bio-Des. Manuf.* **5** 481–96
[38] Tamaddon M, Gilja H, Wang L, Oliveira J M, Sun X, Tan R and Liu C 2020 Osteochondral scaffolds for early treatment of cartilage defects in osteoarthritic joints: from bench to clinic *Biomater. Transl.* **1** 3
[39] Hamzeh S, Miraftab M and Yoosefinejad A 2014 Study of electrospun nanofibre formation process and their electrostatic analysis *J. Ind. Text.* **44** 147–58
[40] Purushothaman A E, Thakur K and Kandasubramanian B 2020 Development of highly porous, electrostatic force assisted nanofiber fabrication for biological applications *Int. J. Polym. Mater. Polym. Biomater.* **69** 477–504
[41] Lim C, Tan E and Ng S 2008 Effects of crystalline morphology on the tensile properties of electrospun polymer nanofibers *Appl. Phys. Lett.* **92** 141908
[42] Alharbi N, Daraei A, Lee H and Guthold M 2023 The effect of molecular weight and fiber diameter on the mechanical properties of single, electrospun PCL nanofibers *Mater. Today Commun.* **35** 105773
[43] Jordan A M and Korley L T 2015 Toward a tunable fibrous scaffold: structural development during uniaxial drawing of coextruded poly (ε-caprolactone) fibers *Macromolecules* **48** 2614–27
[44] D'Amato A R, Schaub N J, Cardenas J M, Franz E, Rende D, Ziemba A M and Gilbert R J 2017 Evaluation of procedures to quantify solvent retention in electrospun fibers and facilitate solvent removal *Fibers Polym.* **18** 483–92
[45] D'Amato A R, Bramson M T K, Corr D T, Puhl D L, Gilbert R J and Johnson J 2018 Solvent retention in electrospun fibers affects scaffold mechanical properties *Electrospinning* **2** 15–28
[46] Schoenenberger A D, Foolen J, Moor P, Silvan U and Snedeker J G 2018 Substrate fiber alignment mediates tendon cell response to inflammatory signaling *Acta Biomater.* **71** 306–17
[47] Cardwell R D, Dahlgren L A and Goldstein A S 2014 Electrospun fibre diameter, not alignment, affects mesenchymal stem cell differentiation into the tendon/ligament lineage *J. Tissue Eng. Regen. Med.* **8** 937–45
[48] Rinoldi C *et al* 2019 Tendon tissue engineering: effects of mechanical and biochemical stimulation on stem cell alignment on cell-laden hydrogel yarns *Adv. Healthc. Mater.* **8** 1801218
[49] Olvera D, Sathy B N, Carroll S F and Kelly D J 2017 Modulating microfibrillar alignment and growth factor stimulation to regulate mesenchymal stem cell differentiation *Acta Biomater.* **64** 148–60
[50] Thayer P S, Verbridge S S, Dahlgren L A, Kakar S, Guelcher S A and Goldstein A S 2016 Fiber/collagen composites for ligament tissue engineering: influence of elastic moduli of sparse aligned fibers on mesenchymal stem cells *J. Biomed. Mater. Res. A* **104** 1894–901
[51] Yi B, Shen Y, Tang H, Wang X and Zhang Y 2020 Stiffness of the aligned fibers affects structural and functional integrity of the oriented endothelial cells *Acta Biomater.* **108** 237–49
[52] Floren M *et al* 2016 Human mesenchymal stem cells cultured on silk hydrogels with variable stiffness and growth factor differentiate into mature smooth muscle cell phenotype *Acta Biomater.* **31** 156–66
[53] Doss B L, Pan M, Gupta M, Grenci G, Mège R-M, Lim C T, Sheetz M P, Voituriez R and Ladoux B 2020 Cell response to substrate rigidity is regulated by active and passive cytoskeletal stress *Proc. Natl Acad. Sci.* **117** 12817–25